Biomaterials Advances 188 (2026) 215025

Contents lists available at ScienceDirect

Biomaterials Advances

journal homepage: www.journals.elsevier.com/materials-science-and-engineering-c

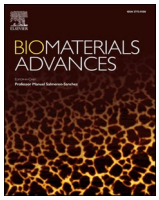

Tannic acid-crosslinked layer-by-layer nanocomposite coatings enhance mechanical stability and pre-osteoblast response in porous polymer-based scaffolds for bone tissue engineering

MohammadAli Sahebalzamani [a,b,c,e,h], John Redmond [a,b,c], Srishti Agarwal [a,b,c], Helen O. McCarthy [d], Tanya J. Levingstone [a,b,c,e,f,g], Nicholas J. Dunne [a,b,c,d,e,f,g,h,i,j,k,*]

[a] School of Mechanical and Manufacturing Engineering, Dublin City University, D09 DD7R, Dublin, Ireland
[b] Centre for Medical Engineering Research, Dublin City University, D09 DEH3, Dublin, Ireland
[c] Biodesign Europe, Dublin City University, D09 V209, Dublin, Ireland
[d] School of Pharmacy, Queen's University Belfast, 97 Lisburn Rd, Belfast, BT9 7BL, United Kingdom
[e] Advanced Manufacturing Research Centre (I-Form), School of Mechanical and Manufacturing Engineering, Dublin City University, D09 NA55, Dublin, Ireland
[f] Tissue Engineering Research Group, Department of Anatomy and Regenerative Medicine, Royal College of Surgeons in Ireland, D02 PN40, Dublin, Ireland
[g] Advanced Processing Technology Research Centre, Dublin City University, D09 NA55, Dublin, Ireland
[h] Research Centre for Medical Devices (CÚRAM), Biomedical Sciences, University of Galway, H91 W2TY, Galway, Ireland
[i] Trinity Centre for Biomedical Engineering, Trinity Biomedical Sciences Institute, Trinity College Dublin, D02 PN40, Dublin, Ireland
[j] Advanced Materials and Bioengineering Research Centre (AMBER), Trinity College Dublin, D02 PN40, Dublin, Ireland
[k] Department of Mechanical and Manufacturing Engineering, School of Engineering, Trinity College Dublin, D02 PN40, Dublin, Ireland

ARTICLE INFO

Keywords:
Layer-by-layer assembly
Multifunctional nanocomposite coatings
Open-cell structures
Chemical crosslinking
Bone tissue-engineering

ABSTRACT

The development of bone tissue-engineered scaffolds requires materials that combine adequate mechanical strength, biocompatibility, and interconnected porosity, while maintaining stability under physiological conditions. However, highly porous polymer-based scaffolds often exhibit reduced mechanical stability in hydrated environments due to water-induced plasticisation. In this study, highly porous polymer-based scaffolds were functionalised using electrostatic Layer-by-Layer (LbL) assembly to enable controlled modification of surface and bulk properties. Multilayer nanocomposite coatings comprising poly-L-lysine, poly-L-glutamic acid, poly(diallyldimethylammonium chloride), and montmorillonite were deposited using LbL assembly. To improve mechanical stability under physiological conditions, the LbL-coated scaffolds were chemically crosslinked using a 1 wt% aqueous tannic acid (TA) solution as a naturally derived green crosslinker.

Physicochemical characterisation was conducted using scanning electron microscopy (SEM), Fourier-transform infrared (FTIR) spectroscopy, X-ray diffraction (XRD), energy-dispersive X-ray (EDX) analysis, and contact angle measurements. SEM analysis confirmed the formation of a uniform and dense multilayer coating following TA crosslinking. Under hydrated conditions (phosphate-buffered saline, PBS, 37 °C), TA-crosslinked scaffolds retained 75% of their dry-state elastic modulus, demonstrating improved mechanical stability. Contact angle measurements showed an increase in surface hydrophilicity, with values decreasing from 138.8 ± 2.85° for uncoated polyurethane to 70.3 ± 3.10° after crosslinking. Biodegradation studies under enzymatic and dynamic conditions showed controlled mass loss (10.5% over 8 weeks), consistent with enhanced structural stability.

In vitro evaluation using MC3T3-E1 pre-osteoblasts confirmed no cytotoxic effects, with cell attachment on crosslinked scaffolds reaching 97.3% ± 2.2% after 24 h. The crosslinked scaffolds supported cell proliferation and maintained favourable cell morphology over 14 days. These results indicate that TA-crosslinked LbL-coated polyurethane scaffolds provide improved mechanical stability, surface properties, and cytocompatibility, supporting their potential use in bone tissue engineering applications.

* Corresponding author at: School of Mechanical and Manufacturing Engineering, Dublin City University, Ireland.
E-mail address: nicholas.dunne@dcu.ie (N.J. Dunne).

https://doi.org/10.1016/j.bioadv.2026.215025
Received 3 February 2026; Received in revised form 22 May 2026; Accepted 16 June 2026
Available online 18 June 2026

1. Introduction

The increasing prevalence of musculoskeletal disorders and injuries has led to a growing demand for bone grafting and replacement materials in clinical settings. These materials must not only restore the structural integrity of damaged bone but also facilitate regeneration and integration with host tissue, making their development essential for improving patient outcomes [1,2]. Advances in bone tissue engineering have focused on designing scaffolds that support effective bone regeneration by providing a suitable environment for cell attachment, proliferation, and differentiation [3,4]. Key requirements for bone scaffolds include appropriate porosity, mechanical strength, and stiffness [5]. However, increasing scaffold porosity to enhance tissue integration often compromises mechanical properties, presenting a significant design challenge [6,7].

Layer-by-Layer (LbL) assembly offers a promising strategy to address this challenge by enabling the deposition of stiff, robust coatings onto highly porous substrates [8]. The process involves the sequential adsorption of oppositely charged polyelectrolytes, resulting in uniform multilayer films with tunable properties [9]. This technique allows for precise control over surface and bulk characteristics and accommodates a wide range of materials, making it particularly suitable for bone tissue engineering applications involving complex, porous structures [9,10]. Previous studies have demonstrated that LbL coatings composed of poly (ethylenimine) (PEI), poly(acrylic acid) (PAA), and montmorillonite (MTM) can significantly enhance the mechanical properties of polymeric scaffolds without compromising porosity [11–14]. For example, our group previously reported that LbL coatings of poly-L-lysine (PLL), poly-L-glutamic acid (PGA), poly(diallyldimethylammonium chloride) (PDDA), and MTM on polyurethane scaffolds increased the compressive modulus from 0.09 ± 0.05 MPa to 3.65 ± 0.70 MPa while maintaining high porosity (86%), a feature critical for bone tissue engineering [15].

Adding a stiff and strong coating through LbL deposition offers a promising solution. This approach can enhance structural integrity while maintaining the necessary porosity for tissue integration [8]. The fabrication of multifunctional, mechanically robust bio-nanocomposite coatings through the LbL assembly technique has gained significant attention for its potential to address key current challenges in bone tissue engineering applications [9,16]. This technique involves sequentially adsorbing oppositely charged electrolyte complexes onto a substrate. LbL assembly achieves the formation of uniform multilayer thin films with tailored properties, allowing for precise surface and bulk functionalisation. One of the benefits of this method is its ability to use multiple materials and functionalities, especially for bone tissue engineering applications on highly porous structures [9,10]. Despite these improvements, most assessments of LbL-coated scaffolds have been conducted under ambient conditions, which do not reflect the hydrated environments encountered *in vivo* [11–15].

Open-cell polyurethane (PU) foams have been widely studied for bone tissue engineering due to their tuneable porous architecture, elasticity, low cost, and ease of fabrication [17,18]. They are commonly used as 3D-porous templates to tailor the physicochemical and mechanical properties of porous bone scaffolds through a LbL coating process [9]. However, several limitations hinder their clinical translation. A key challenge is the inherent trade-off between porosity and mechanical strength: although high porosity and the interconnected pores are essential for cell infiltration, vascularisation, and nutrient transport, they reduce the load-bearing capacity and structural stiffness of the scaffold [19]. In addition, PU scaffolds are also sensitive to water, which acts as a plasticiser, leading to swelling and reduced stiffness [20]. Consequently, while LbL coatings improve mechanical properties under dry conditions, these benefits decrease in hydration environments, where scaffolds exhibit hydrogel-like behaviour and limited reinforcement [21,22]. This highlights the need to characterise scaffold performance under physiologically relevant hydrated conditions [23]. Improving mechanical stability in such environments while limiting water-induced plasticisation would enhance their suitability for bone tissue applications [24]. In addition, controlling the degradation behaviour remains challenging, as PU degradation depends on hydrolytic and enzymatic processes that are sensitive to local environmental conditions, often resulting in variable mass loss and structural instability [25]. Therefore, strategies that can maintain high porosity while improving mechanical stability and enabling controlled degradation under physiological conditions are required for the effective application of PU scaffolds in bone tissue engineering.

Crosslinking is widely used to improve the performance of polymeric systems, including hydrogels and polyelectrolyte multilayers, under hydrated conditions relevant to biomedical applications [26,27]. Studies on model systems, such as poly(styrene sulfonate) (PSS) and PDDA, have examined the effects of hydration and relative humidity on multilayer films, polyelectrolyte complexes, and nacre-like composites [28], but have largely provided qualitative insights, with little quantitative analysis of mechanical properties, water uptake and degradation behaviour in LbL coated systems. Chemical crosslinking, typically using agents such as carbodiimides (*e.g.*, EDAC), genipin, or GA, enhances stability and mechanical strength by forming covalent bonds between polymer chains is an effective method to increase the stability and mechanical strength of polymeric materials by forming covalent bonds between polymer chains [9,14,29–31]. However, crosslinking of LbL coatings on PU-based scaffolds for bone tissue engineering remains insufficiently studied. Ziminska et al. (2016) reported that thermal crosslinking of PEI/PAA/PEI/MTM coatings improved cell viability and coating stability compared to non-crosslinked controls [32], while Acheson et al. (2023) showed that GA crosslinking reduced water-induced plasticisation, enabling retention of approximately 56% of mechanical properties under hydrated conditions [14]. Despite these advances, the effects of GA crosslinking on cellular responses and scaffold degradation rates are not well defined.

The enhanced retention of mechanical properties arises from the combined contribution of multiple intermolecular interactions [9]. Electrostatic interactions between fully charged species drive the assembly of polyelectrolyte-based LbL coatings, while secondary interactions, particularly hydrogen bonding between partially charged groups, further stabilise the structure. In systems containing functional groups such as –OH, –COOH, and –NH_2, hydrogen bonding contributes significantly to cohesion and resistance to mechanical instability [9,15].

A major limitation of many chemical crosslinkers is their potential cytotoxicity, which is often concentration-dependent [33–35]. Natural crosslinkers such as genipin and tannic acid (TA) offer safer alternatives with lower cytotoxicity [30,36]. TA, a polyphenolic compound ($C_{76}H_{52}O_{46}$), can form multiple bonds with biomacromolecules, enhancing the mechanical properties and stability of tissue-engineered scaffolds [37]. It has also been reported that TA can impart antibacterial properties and modulate scaffold degradation, swelling, and cell-material interactions [37,38]. For example, the incorporation of TA into chitosan scaffolds increased mechanical strength and Young's modulus, and its hydroxyl groups influenced wettability and cell attachment [39]. The antimicrobial activity of TA can be tuned by adjusting its concentration and environmental conditions [33,38], making it an attractive “green” crosslinker for biomedical applications [37]. In a previous study, chitosan scaffolds were crosslinked with 1% GA and 1% TA to compare cytotoxicity and mechanical properties [37]. The results indicated that TA interacted with chitosan through hydrophobic and hydroxyl groups, whereas GA formed covalent bonds with the amino groups of the chitosan scaffold. TA crosslinking increased the scaffold's mechanical strength to 25 MPa, compared to approximately 13 MPa for uncrosslinked chitosan [37]. The hydroxyl groups in TA also influenced wettability, which can affect protein adsorption and cell attachment [37]. However, studies on TA crosslinking in nanocomposite layer-by-layer (LbL) coatings remain limited, particularly regarding hydration effects on mechanical properties and water uptake in highly porous scaffolds. To date, no work has systematically examined the use

of novel crosslinkers in multifunctional PLL/PGA/PDDA/MTM LbL coatings on open-cell polymer foam scaffolds, nor their impact on *in vitro* cellular response and biodegradation in bone tissue applications.

Specifically, TA forms hydrogen bonds with the amine and carboxyl groups of PLL and PGA, engages in electrostatic interactions with charged polyelectrolytes such as PDDA, and establishes coordination interactions with the inorganic MTM nanoclay [14,37]. Together, these interactions increase crosslinking density, limit polymer chain mobility, and strengthen interfacial cohesion within the multilayer structure. This reduces water-induced plasticisation and improves mechanical stability under hydrated conditions [38].

This study aims to evaluate the effectiveness of TA crosslinking in maintaining the mechanical and physicochemical properties of LbL-coated porous polyurethane foam-based scaffolds under hydrated conditions, with a focus on their suitability for bone tissue engineering applications (Fig. 1). We further assess the *in vitro* degradation of TA-crosslinked LbL-coated scaffolds under enzymatic and dynamic conditions, as well as their biocompatibility, cell attachment, proliferation, morphology, and cellular responses using MC3T3-E1 pre-osteoblasts.

2. Materials and methods

2.1. Scaffold materials and preparation

Nanocomposite LbL-coated scaffolds were fabricated using open-cell polyurethane foam-based scaffolds (10 mm diameter × 12 mm height, 45 pores per inch (PPI); EasyFoam Ltd., UK). Polyelectrolyte solutions included 1 wt% poly-L-lysine (PLL, M_w: 182.65 g/mol), poly-L-glutamic acid (PGA, M_w 147.13 g/mol), poly(diallyldimethylammonium chloride) (PDDA, M_w 400 kDa, 20 wt% in H_2O; Sigma Aldrich, Ireland), and 0.5 wt% montmorillonite (MTM, Cloisite Na^+, D_{50} of <25 μm; BYK, UK). Solutions were prepared in deionised (DI) water (resistivity ≥18.2 MΩ·cm), stirred for 24 h, and pH-adjusted as described previously [15]. The polymer-based scaffolds were cleaned by immersion in 1 M NaOH (10 min), rinsed with DI water, and desiccated for 24 h before LbL coating.

2.2. Layer-by-layer (LbL) assembly

Scaffolds were coated using a dynamic LbL assembly process in a custom chamber, combining perfusion (12 mL/min, 10 rpm) and cyclic compressive loading (5% strain, 1 Hz) [15]. Each quadlayer consisted of sequential immersion in PLL (+), PGA (−), PDDA (+), and MTM (−) solutions for 30 s each, with three 30 s DI water rinses between each layer [12,15]. This process was repeated to deposit 10 quadlayers. A minimum of 10 quadlayers was selected based on our previous study, which showed that this deposition level was sufficient to demonstrate an optimal improvement in LbL-coated scaffold properties [15]. After coating, scaffolds were rinsed three times with DI water and dried in a desiccator (10% RH, 24 h) before characterisation. The experimental conditions, including LbL coating parameters (coating method, deposition time, and processing conditions) and material parameters (solution concentrations, pH, and scaffold pore size), were selected based on our recently published optimisation study using a design of experiments approach, which identified conditions yielding optimal performance in comparable systems [40].

2.3. Crosslinking

The LbL-coated scaffolds were immersed in a 1 wt% TA solution (Sigma-Aldrich, Ireland) for 12 h at 22 °C (unadjusted pH), based on previous studies demonstrating effective crosslinking of polyelectrolyte systems at this concentration [33,37,41]. After crosslinking, scaffolds were washed five times in DI water (3 min each) to remove unbound TA, then dried in a desiccator for 48 h before analysis.

2.4. Physico-chemical and mechanical characterisation

2.4.1. Scanning electron microscopy

Scaffold morphology and coating uniformity were analysed using a Zeiss EVO LS15 SEM (18 kV accelerating voltage). Samples ($n = 3$ per group) mounted on aluminium discs were sputter-coated with gold (60 mA, 80 s; Edwards System). Pore size was quantified from SEM images using ImageJ (v1.8.0_172; NIH, USA) with measurements taken from scanning electron microscopy (SEM) images captured at ×1000 magnification. Five images per sample were randomly selected and analysed for each group [15]. The coating thickness was determined from 10 measurements obtained from at least four SEM images captured from different regions of each scaffold [15].

2.4.2. Porosity

Gravimetric porosity was measured using a Sartorius LA 620P Top-loader scale balance (Sartorius Ltd., UK) with a YDL01 density determination kit in ambient and hydrated conditions ($n = 3$). Scaffold density (ρ_s) was calculated from dimensions (vernier calliper) and mass, and determined as:

$$\rho_s = \frac{\text{Mass of Scaffold (g)}}{\text{Volume (m}^3\text{)}}$$

Subsequently, the porosity was determined as:

$$\text{Porosity (\%)} = \left[1 - \left(\frac{\rho_s}{\rho_m}\right)\right] \times 100$$

where ρ_s is the measure scaffold density and $\rho_m = 1.20$ g/cm^3 (theoretical density of the polyurethane) [42].

2.4.3. Mechanical testing

Uniaxial compression tests were performed using a CellScale BioTester (Univert, Canada; 100 N load cell, $n = 3$) to 0.6 mm deformation at 2 mm/min with a 0.03 N preload. The compressive modulus was

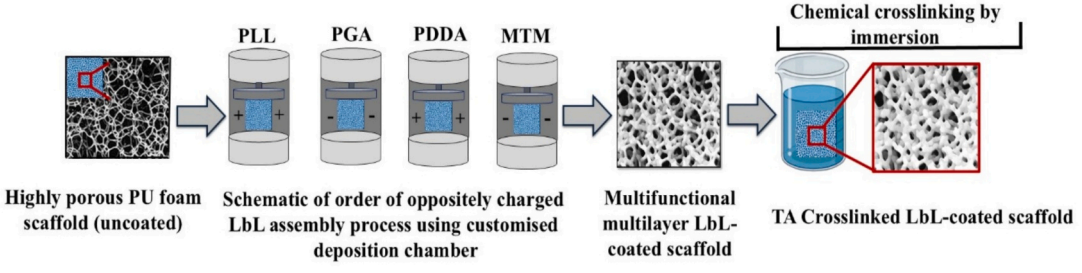

Fig. 1. Schematic representation of the layer-by-layer (LbL) assembly process and tannic acid (TA) crosslinking. The diagram illustrates sequential deposition of poly-L-lysine (PLL), poly-L-glutamic acid (PGA), poly(diallyldimethylammonium chloride) (PDDA), and montmorillonite (MTM) onto a porous polyurethane foam-based scaffold, followed by TA crosslinking. This process produces a multifunctional nanocomposite coating designed to enhance scaffold performance for bone tissue engineering applications.

calculated from the linear region of the stress-strain curve. Mechanical testing was performed under dry and hydrated (phosphate-buffered saline (PBS), 37 °C) conditions.

2.4.4. Attenuated total reflectance-Fourier-transform infrared spectroscopy

Attenuated total reflectance-Fourier-transform infrared (ATR-FTIR) spectra were acquired (PerkinElmer Spectrum 100, USA) for each group ($n = 3$), scanning 500–4000 cm^{-1} (64 scans/sample). Spectra were normalised, and characteristic functional groups were identified.

2.4.5. X-ray diffraction

X-ray diffraction (XRD) (Bruker D8, Germany; 30 kV, 10 mA; 2θ = 20–80°; Cu-Kα radiation) was used to confirm nanoclay incorporation ($n = 5$). Peaks were identified using the JCPDS database and X'Pert High Score Plus software (Netherlands).

2.4.6. Energy dispersive X-ray

Elemental composition was assessed by scanning electron microscopy with energy dispersive X-ray (SEM-EDX) analysis (Zeiss EVO LS15, Germany) at five locations per sample ($n = 3$).

2.4.7. Water contact angle

Hydrophobicity was assessed by sessile drop (5 μL DI water) using an FTÅ200 Dynamic Contact Angle Analyser (First Ten Angstroms, USA; n = 3). Contact angles were averaged from multiple positions ($n = 5$) on the surface of each sample.

2.5. In vitro degradation

Scaffolds (uncoated, LbL-coated, crosslinked LbL-coated; n = 3) were sterilised in 70% ethanol (10 min), rinsed in sterile PBS, and incubated at 37 °C, 60 RPM in PBS or PBS with lysozyme (13 mg/L, Fisher Scientific, Ireland) and lipase (110 U/L, Sigma-Aldrich, Ireland) to simulate physiological degradation [43]. Enzyme solutions were refreshed every 48 h [44]. At each time point (Day 7, 14, 21, 28, 35, 42, 49, 56), scaffolds were weighed using an analytical balance (METTLER AT261, Mettler Toledo, Belgium), dried (24 h, desiccator), and mass loss calculated. Morphological changes were assessed by SEM-EDX. Water uptake and pH of the degradation medium were also recorded.

2.5.1. Weight loss

The weight loss (%) following degradation ($n = 3$) was calculated as:

$$\text{Weight Loss}\ (\%) : \frac{W_0 - W_d}{W_0} \times 100$$

where W_0 is the initial dry weight, and W_d is the dry weight after the degradation period [45].

2.5.2. Swelling ratio

The swelling ratio (%) was determined to infer the absorption capacity of the scaffolds (n = 3):

$$\text{Swelling ratio}(\%) : \frac{W_s - W_d}{W_d} \times 100$$

where W_s is the swollen weight (after blotting excess surface water), and W_d is the dry weight [33,45].

2.5.3. pH monitoring

Medium pH was measured at each time point during *in vitro* degradation using a calibrated pH meter (WTW inoLab pH 720, Germany) before solution changes.

2.6. In vitro biocompatibility assessment

2.6.1. Cell culture

Scaffolds (uncoated, LbL-coated, crosslinked LbL-coated; $n = 5$) were cut to ~10 × 6 mm, equilibrated in PBS (1 h), sterilised in 70% ethanol (15 min), and washed in sterile PBS [46]. MC3T3-E1 pre-osteoblasts (Merck Life Science, Ireland) were cultured in αMEM with 10% foetal bovine serum (FBS, Thermo Fisher, UK) and 1% PenStrep (Sigma-Aldrich, Ireland) at 37 °C, 5% CO_2. Cells were passaged with 0.25% trypsin and counted by trypan blue exclusion.

2.6.2. Cytotoxicity (MTT assay)

Cytotoxicity was assessed according to ISO 10993-5 using the MTT assay (Thermo Fisher Scientific, Ireland). Scaffolds were incubated in sterilised scaffolds in αMEM for 24 h to allow leachable substances to diffuse into the medium. MC3T3-E1 cells were seeded at 1×10^5 cells/well in 24-well plates and exposed to these conditions. Stainless steel and natural rubber latex served as negative and positive controls, respectively. After 24 and 48 h exposure, MTT solution (0.5 mg/mL) was added for 4 h, formazan dissolved in DMSO, and absorbance was measured at 540 nm (Infinite 200 PRO, TECAN, Switzerland). The cell viability (%) was determined as

$$\text{Cell Viability}\ (\%) : \frac{\text{Sample Absorbance}_{540nm}}{\text{Mean Negative Control Absorbance}_{540nm}} \times 100$$

2.6.3. Scaffold seeding

Sterilised scaffolds were pre-incubated overnight in αMEM with 50% FBS at 37 °C and 5% CO_2. MC3T3-E1 cells were seeded (5×10^4 per scaffold) using a double-sided technique, allowed to attach for 1 h, and then cultured in 1.5 mL medium with media changes every 2–3 days.

2.6.4. Cell attachment

After overnight incubation, scaffolds ($n = 3$) were rinsed in PBS to remove non-adherent cells. The attached cells were quantified using the CyQUANT™ Cell Proliferation Assay (Invitrogen, C7026), comparing DNA content to a standard curve. The extent of cell attachment (%) was determined as:

$$\text{Cell Attachment}\ (\%) : \frac{\text{Number cells attached}}{\text{Number of cells seeded}} \times 100$$

2.6.5. Cell proliferation

Cell proliferation was assessed at Days 1, 4, 7, and 14 using the alamarBlue assay. Seeded scaffolds were incubated with 10% alamarBlue in DMEM for 4 h; absorbance was measured at 570 and 600 nm using an Infinite 200 PRO plate reader (Tecan Trading AG, Switzerland). Unseeded scaffolds served as the negative control group.

2.6.6. Cell morphology (SEM)

At Days 1, 7, and 14, scaffolds were fixed in 2.5% glutaraldehyde (overnight, 4 °C), dehydrated in graded ethanol, treated with hexamethyldisilazane, dried, and imaged by SEM (as per §2.4.1) using an accelerating voltage of 5 kV.

2.6.7. Live/dead viability

Live/Dead staining was performed using the LIVE/DEAD™ Viability/Cytotoxicity Kit (Invitrogen, L3224). Scaffolds were incubated with 1 μM calcein-AM and 2 μM ethidium homodimer-1 for 30 min at 37 °C. Between 3 and 6 images were captured using an EVOS FL system (Thermo Fisher Scientific, UK) at excitation/emission wavelengths of 495/515 nm for calcein and 528/617 nm for ethidium homodimer-1.

2.6.8. Statistical analysis

All experiments were performed with a minimum of three replicates per group. Data are presented as mean ± standard deviation (SD). One-way ANOVA was used for comparisons involving multiple groups, and

independent sample *t*-tests were applied for pairwise comparisons where appropriate (GraphPad Prism v8.0.2). A *p*-value <0.05 was considered statistically significant. Significance levels are indicated as *p-value ≤0.05, **p-value ≤0.01, ***p-value ≤0.001.

3. Results

3.1. Physico-chemical and mechanical characterisation

3.1.1. Scanning electron microscopy analysis

SEM imaging showed distinct differences in surface and internal morphology among the three scaffold groups: uncoated polyurethane foam, LbL-coated (uncrosslinked), and TA crosslinked LbL-coated scaffolds. The TA crosslinked scaffolds exhibited a denser and more uniform multilayer coating compared to the uncrosslinked LbL group, with improved coating consistency and reduced pore size and porosity (Fig. 2). This densification, typical of crosslinked networks, is associated with enhanced mechanical stability [47]. Quantitative measurements of coating thickness, pore size range, and porosity for all groups are summarised in Table 1.

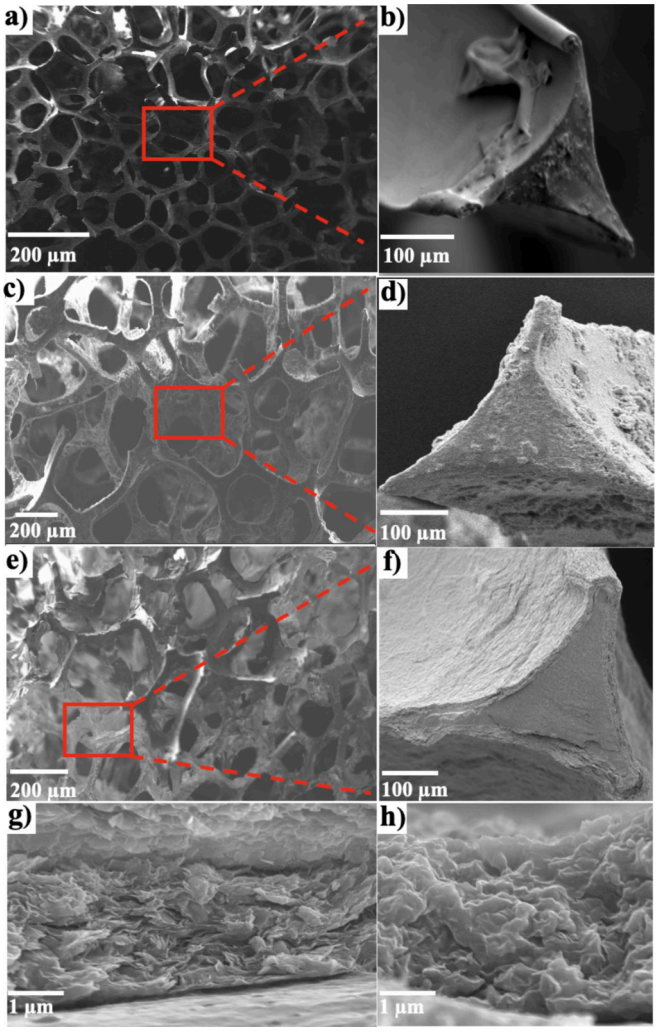

Fig. 2. SEM images of the scaffold surface morphology and pore architecture: (a, b) uncoated, (c, d) LbL-coated (uncrosslinked), (e, f) TA-crosslinked LbL-coated, and (g, h) cross-sectional views of the TA-crosslinked LbL-coated scaffold, showing the multilayered coating, incorporation of nanoclay sheets and interfacial integration after crosslinking. The images show uniform deposition of 10 quadlayers while preserving the open-cell porous architecture.

Table 1
Morphological characteristics of uncoated, LbL-coated (uncrosslinked), and TA-crosslinked LbL-coated scaffold types, including coating thickness, pore size range, and total porosity. Data are presented as mean ± standard deviation (n = 3).

Scaffold type	Coating thickness (µm)	Porosity size range (µm)	Porosity (%)
Uncoated scaffold	–	119–581	97.40 ± 0.70
Uncrosslinked LbL-coated scaffold	1.80 ± 0.65	125–494	95.65 ± 0.55
TA-crosslinked LbL-coated scaffold	2.70 ± 0.80	110–442	94.85 ± 0.90

3.1.2. Mechanical properties

Mechanical testing under both ambient and hydrated conditions demonstrated significant differences between groups. The compressive modulus of uncoated polyurethane scaffolds was 85.1 ± 5.7 kPa, which increased to 562.3 ± 15.2 kPa after LbL coating with 10 quadlayers of PLL/PGA/PDDA/MTM (*p*-value ≤0.001), representing an improvement in mechanical performance [15]. However, under hydrated conditions (PBS, 37 °C), the compressive modulus of LbL-coated scaffolds decreased to 130.1 ± 12.4 kPa due to water-induced plasticisation. TA crosslinking mitigated this effect, resulting in a hydrated compressive modulus of 423 ± 18.9 kPa, with crosslinked scaffolds retaining approximately 75% of their dry-state mechanical properties (Fig. 3). No significant loss in mechanical integrity was observed after pre-hydration in PBS for up to 24 h, indicating stable crosslinking and suitability for *in vivo* applications.

3.1.3. Attenuated total reflectance-Fourier-transform infrared spectroscopy

ATR-FTIR spectra confirmed the chemical composition of all scaffold groups (Fig. 4). The crosslinked LbL-coated scaffolds displayed enhanced peak intensities for the amide and hydroxyl groups, indicating the formation of stable chemical bonds and increased coating integrity. Notable peaks included amide A (~3300 cm^{-1}, N—H stretching), amide I (~1635 cm^{-1}, C═O stretching), and amide II (~1550 cm^{-1}, N—H bending), consistent with successful crosslinking.

3.1.4. X-ray diffraction analysis

XRD analysis further confirmed the incorporation of TA into the LbL nanocomposite coating (Fig. 5). The crosslinked scaffolds exhibited five distinct peaks at approximately 20.85°, 27.68°, 35.72°, 54.43°, and 62.53°, indicative of a well-ordered, layered structure. These peaks were identified as Na—Si (JCPDS #96-153-4381) and SiO_2 (JCPDS #00-033-1161) phases, consistent with the presence of nanoclay and tannate phases reported in previous studies [48,49].

3.1.5. Energy dispersive X-ray analysis

EDX analysis confirmed the elemental composition of the scaffolds. The presence of MTM in LbL-coated scaffolds was evidenced by characteristic elements such as aluminium (4.95%, sodium (2.42%), and silicon (10.66%). After TA crosslinking, an increase in carbon and oxygen content of 3% and 15%, was observed, consistent with the incorporation of tannic acid (Fig. 6).

3.1.6. Contact angle analysis

Water contact angle measurements demonstrated changes in surface wettability following LbL coating and crosslinking. Uncoated polyurethane scaffolds were highly hydrophobic (water contact angle = 138.8° ± 2.85), while LbL coating reduced the water contact angle to 107.7° ± 3.67. TA crosslinking further decreased the water contact angle to 70.3° ± 3.10, indicating increased hydrophilicity (Fig. 7). The significant reduction in water contact angle following crosslinking ($p \leq 0.001$) supports improved surface compatibility for cell attachment.

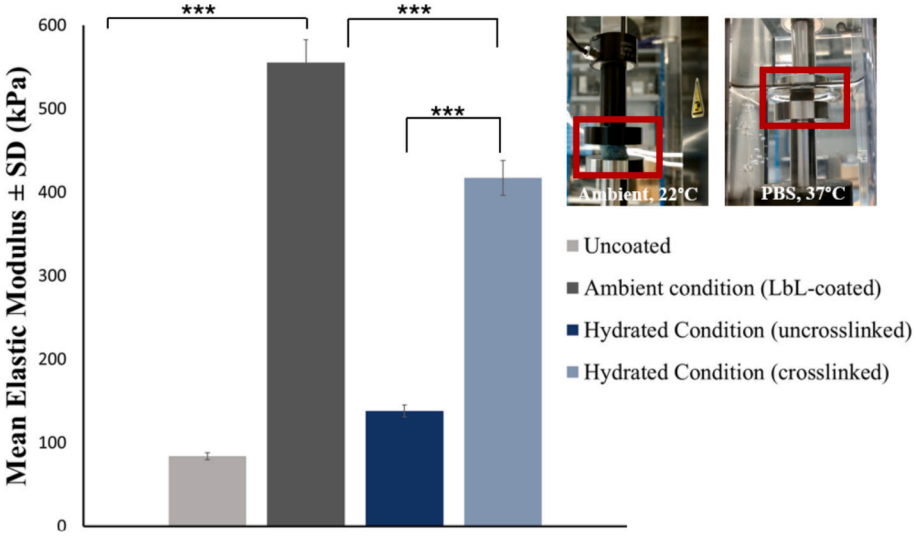

Fig. 3. Compressive modulus of scaffolds measured under dry and hydrated conditions. Comparison between uncoated, LbL-coated (uncrosslinked), and TA-crosslinked LbL-coated scaffold types in physiological environments. Data are presented as mean ± standard deviation ($n = 3$). *** denotes a p-value <0.001.

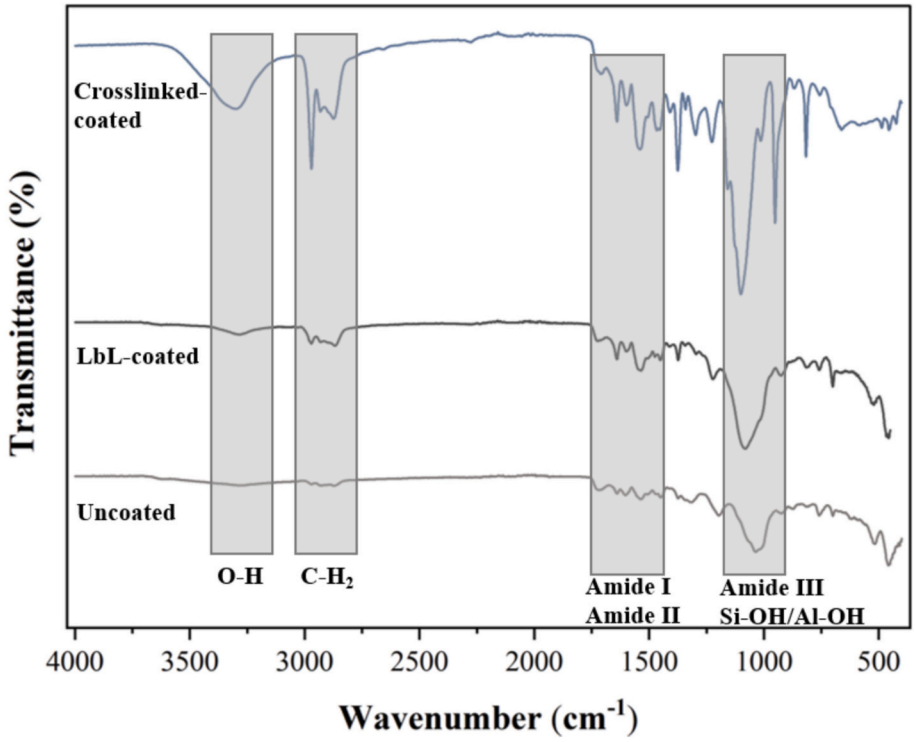

Fig. 4. Attenuated Total Reflectance-Fourier-Transform Infrared spectra of uncoated, LbL-coated (uncrosslinked), and TA-crosslinked LbL-coated scaffold types. Characteristic absorption bands corresponding to each component and crosslinking are indicated. Spectra are normalised for comparison.

3.2. *In vitro degradation properties*

The *in vitro* degradation of all scaffold groups was assessed over 56 days at 37 °C, under agitation, in both PBS and PBS supplemented with lysozyme and lipase enzymes. The pH of the degradation medium remained stable (7.01–7.39 in PBS; 6.75–7.4 in enzyme-supplemented PBS), indicating minimal acidification or basicity changes during degradation (Fig. 8a and Fig. 9a). Water uptake after 8 weeks was 156% for uncoated, 127% for uncrosslinked LbL-coated, and 91% for crosslinked LbL-coated scaffolds, with enzyme exposure increasing swelling in all groups (Fig. 8b and Fig. 9b).

No appreciable degradation was observed in the PBS alone for any group (Fig. 8c). In contrast, enzymatic conditions significantly accelerated degradation rates (p-value ≤0.001). Mass loss after 56 days was 19.2% for uncoated, 14.6% for uncrosslinked LbL-coated, and 10.5% for crosslinked LbL-coated scaffolds (Fig. 9c). The crosslinked scaffolds exhibited the slowest degradation rate, indicating enhanced stability. SEM imaging at 4 and 8 weeks showed that all scaffolds largely maintained their interconnected porous structure, with minimal surface defects (Fig. 10).

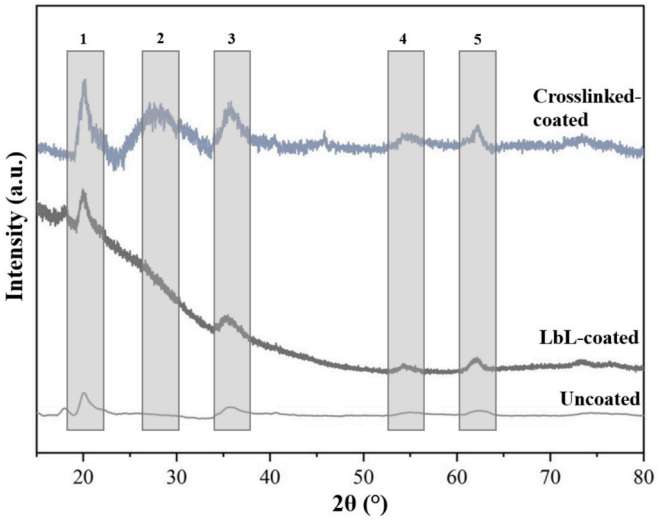

Fig. 5. X-ray diffraction patterns of uncoated, LbL-coated (uncrosslinked), and TA-crosslinked LbL-coated scaffold types. Peaks corresponding to montmorillonite (peaks number 2 and 3) and changes in crystallinity after coating and crosslinking are highlighted.

3.3. *In vitro biocompatibility assessment*

3.3.1. *Cytotoxicity*

Cytotoxicity was evaluated using the ISO 10993-5 extraction method with MC3T3-E1 pre-osteoblasts. All scaffold extracts demonstrated cell viabilities ≥100% after 48 h, exceeding the ISO threshold of 70% [50] (Fig. 11a). Crosslinked scaffolds showed the highest viability (114%), with no significant reduction observed in any group compared to the negative control, indicating the absence of cytotoxic leachates.

3.3.2. *Cell attachment*

Cell attachment efficiency, assessed 24 h post-seeding, exceeded 80% for all groups. Crosslinked scaffolds supported the highest attachment (97.3% ± 2.2%), followed by uncoated (88.2% ± 4.2%) and uncrosslinked LbL-coated scaffolds (80.8% ± 3.1%) (Fig. 11b).

3.3.3. *Cell proliferation*

Cell proliferation, measured by alamarBlue reduction, increased over 14 days in all groups. The crosslinked scaffolds exhibited a continuous increase in metabolic activity, with alamarBlue reduction rising from 17.2% on Day 1 to 35.5% on Day 14 (p-value ≤0.001), indicating robust cell growth (Fig. 11c). In contrast, uncoated and uncrosslinked scaffolds showed lower proliferation rates.

3.3.4. *Cell morphology and fluorescence staining*

SEM analysis demonstrated that MC3T3-E1 cells attached and spread across all scaffold groups, with increasing cell density observed over time (Fig. 12). By Day 14, crosslinked scaffolds exhibited dense cell aggregates and extensive filopodia, indicating strong cell-cell and cell-

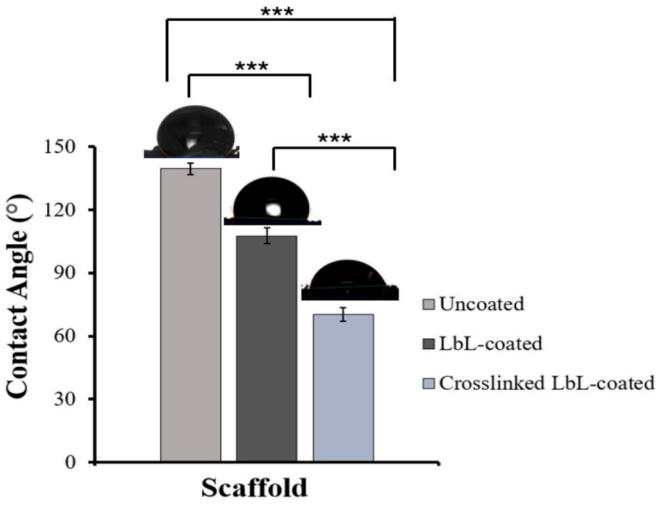

Fig. 7. Water contact angle measurements for the uncoated, LbL-coated (uncrosslinked), and TA-crosslinked LbL-coated scaffold types. Data are presented as mean ± standard deviation (n = 3). *** denotes a p-value <0.001.

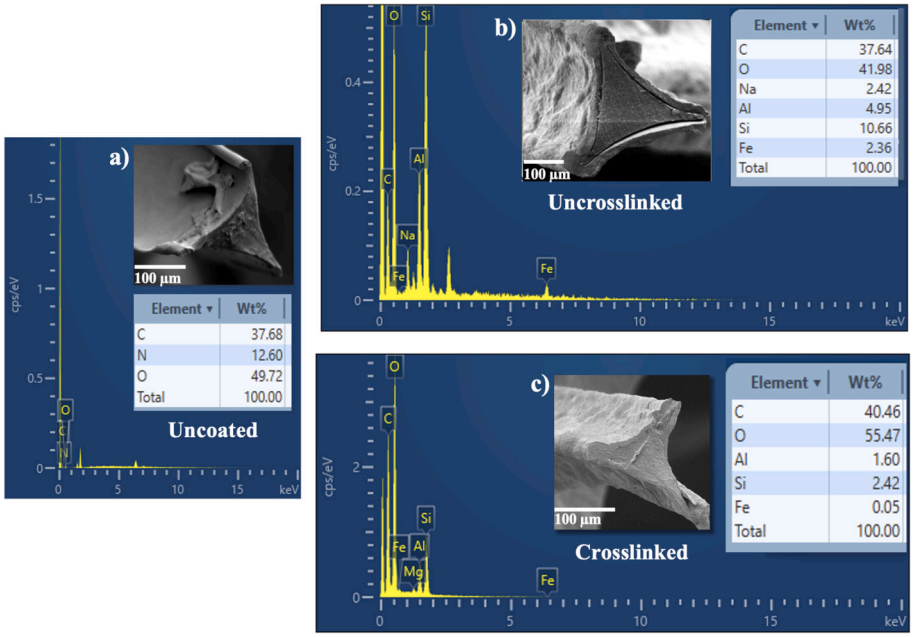

Fig. 6. Scanning Electron Microscopy with Energy Dispersive X-Ray elemental mapping of uncoated, LbL-coated (uncrosslinked), and TA-crosslinked LbL-coated scaffold types. Distribution of key elements (C, N, O, Cl, Na, Si, Al) confirms uniform incorporation of polyelectrolytes and montmorillonite within the multilayer coating.

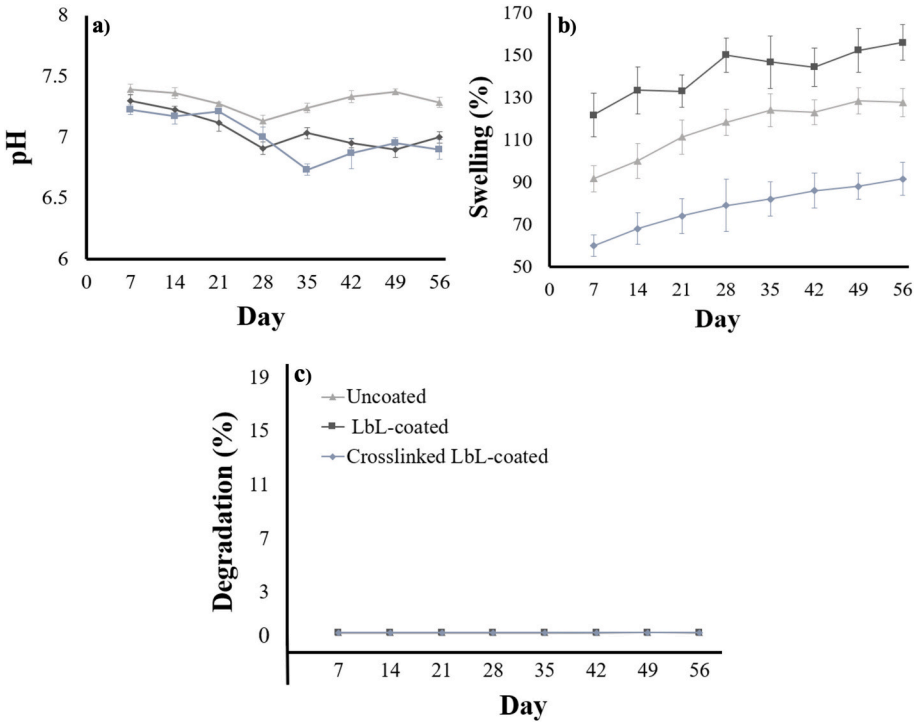

Fig. 8. *In vitro* non-enzymatic degradation behaviour of uncoated, LbL-coated (uncrosslinked), and TA-crosslinked LbL-coated scaffold types over 8 weeks. (a) pH variation of the incubation medium, monitored weekly, indicating changes in scaffold degradation by-products. (b) The swelling ratio of scaffolds, measured at each time point, reflects water uptake and hydration capacity throughout the study period. (c) Degradation rate (%), calculated as the percentage of initial scaffold mass lost over time. Data are presented as mean ± standard deviation ($n = 3$).

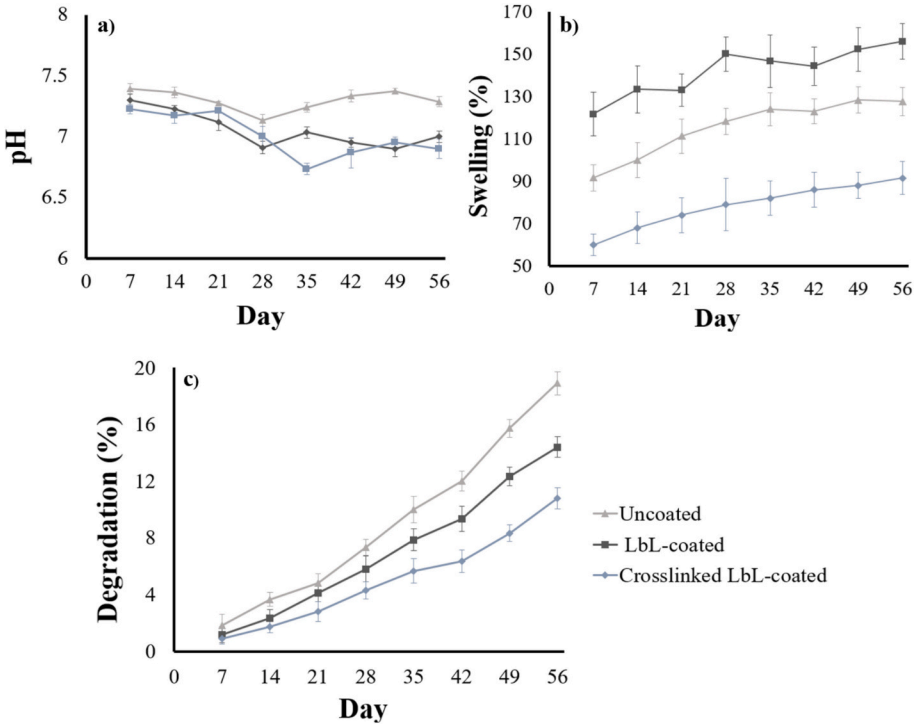

Fig. 9. *In vitro* enzymatic degradation behaviour of uncoated, LbL-coated (uncrosslinked), and TA-crosslinked LbL-coated scaffold types. (a) pH of the degradation medium was measured at each time point, indicating changes associated with scaffold degradation. (b) Swelling ratio (%), representing the percentage increase in scaffold mass due to water uptake during incubation. (c) Degradation rate (%), calculated as the percentage of initial scaffold mass lost over time. Data are presented as mean ± standard deviation (n = 3).

matrix interactions. Cells on crosslinked scaffolds formed a uniform layer within the interconnected pore network. Live/Dead fluorescence staining at Day 1 and Day 7 confirmed high cell viability on all scaffolds, with the crosslinked group displaying the highest proportion of live

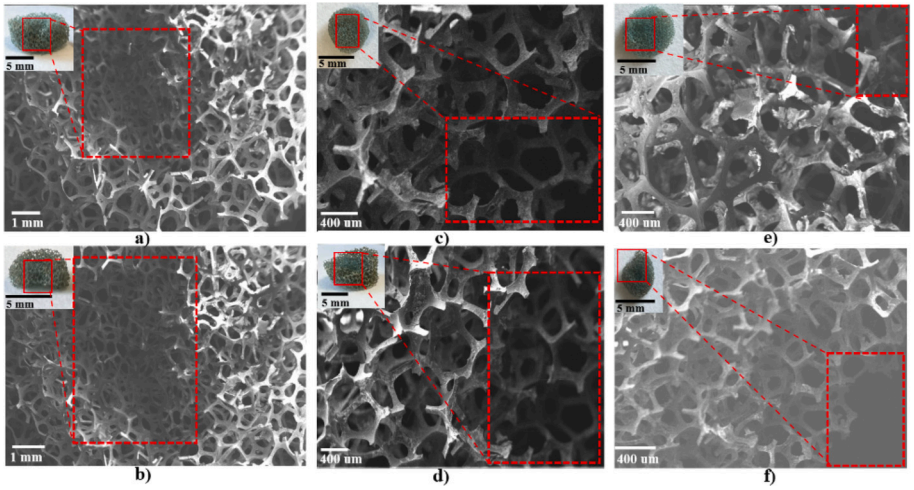

Fig. 10. SEM images illustrating the biodegradation of the polyurethane scaffolds over time. Images depict changes in surface appearance and microstructure at Day 28 (top row) and Day 56 (bottom row) for: (a, b) uncoated, (c, d) LbL-coated (uncrosslinked), and (e, f) TA-crosslinked LbL-coated scaffold types. Red lines highlight regions exhibiting visible degradation within the interconnected scaffold architecture.

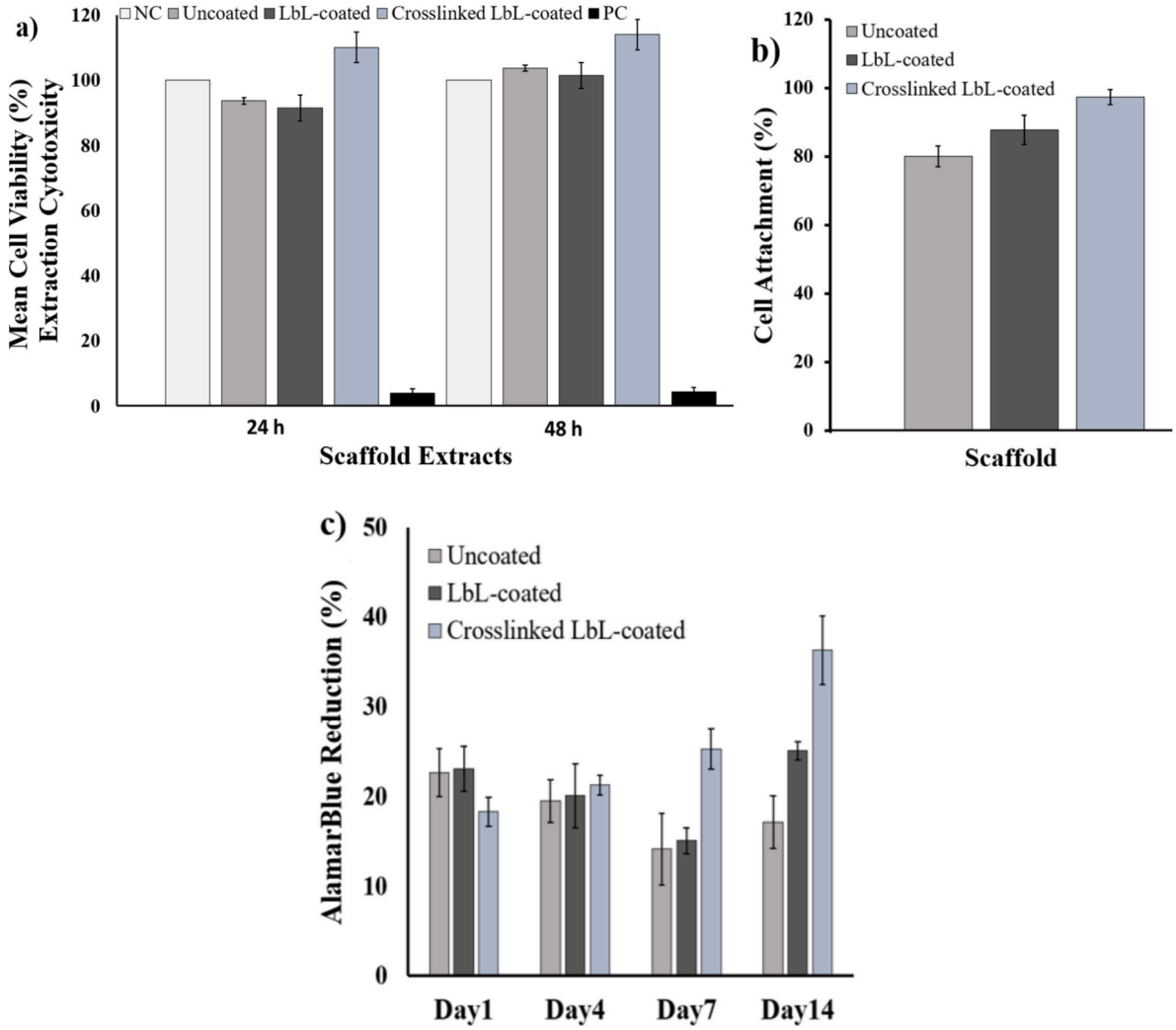

Fig. 11. *In vitro* biological evaluation of uncoated, LbL-coated (uncrosslinked), and TA-crosslinked LbL-coated scaffold types: (a) MC3T3-E1 cells cultured with scaffold extracts for 48 h exhibited no cytotoxic response, with cell viability remaining at approximately 100% for all scaffold types. NC: negative control; PC: positive control. (b) Cell attachment to all scaffold types after 24 h ranged from 80% to 97%, with no statistically significant differences observed among scaffold types. (c) AlamarBlue reduction, used to assess cell proliferation over 14 days, showed a continuous increase in metabolic activity for the TA-crosslinked scaffold type. Data are presented as mean ± standard deviation ($n = 4$).

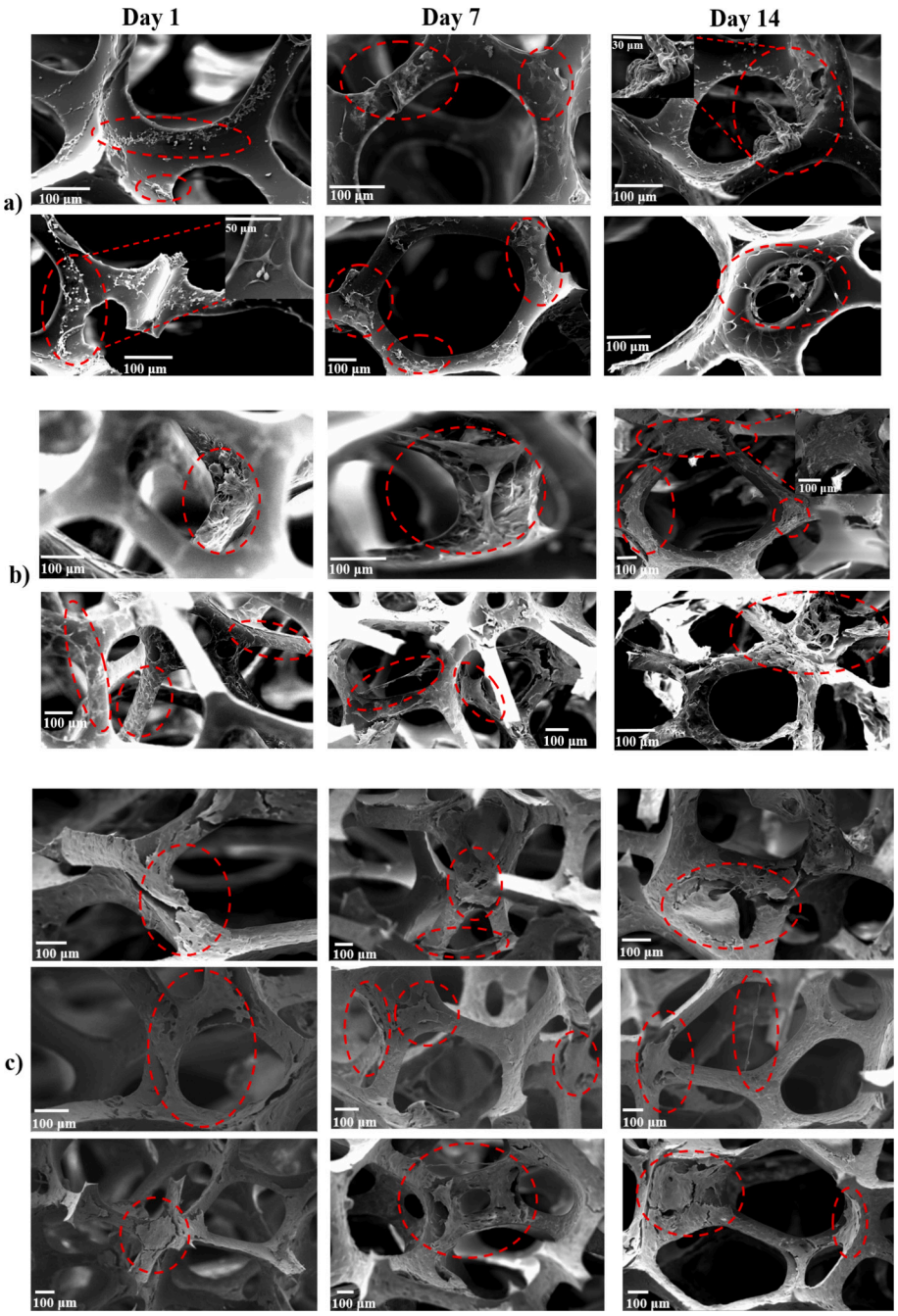

Fig. 12. SEM images of dehydrated MC3T3-E1 cell-scaffold constructs at Days 1, 7, and 14, illustrating cell morphology, attachment and spatial distribution within (a) uncoated, (b) LbL-coated (uncrosslinked), and (c) TA-crosslinked LbL-coated scaffold types.

(calcein-AM positive) cells and minimal necrosis (Fig. 13). The crosslinked scaffolds consistently supported greater cell survival and spreading compared to the other groups.

4. Discussion

The development of multiscale polymer-based scaffolds that combine suitable biological and mechanical properties with high interconnectivity is essential for clinical translation in bone tissue engineering [51]. LbL assembly offers a versatile method for modifying both the surface and bulk properties of scaffolds, enabling tailored tuning of their functional characteristics [9]. In this study, we used TA as a green crosslinker for LbL-assembled, highly porous polyurethane scaffolds, addressing the cytotoxicity concerns associated with conventional crosslinkers such as glutaraldehyde [52].

The LbL assembly of PLL, PGA, PDDA, and MTM onto open-cell polymer-based scaffolds resulted in a nanocomposite-based layered coating that enhanced the physical, mechanical, chemical, and biological properties of the scaffolds. TA crosslinking led to a more homogeneous and robust nanocomposite coating, as confirmed by SEM, with improved structural uniformity compared to uncrosslinked LbL coatings. This stabilising effect is consistent with previous studies on the ability of TA to improve the morphology and mechanical strength of protein-based films [27]. Although crosslinking led to a slight reduction in porosity and pore size, the scaffolds retained high interconnectivity, which is critical for bone tissue engineering applications [15].

Mechanical testing demonstrated that LbL coating substantially increased the elastic modulus of the polymer-based scaffolds under

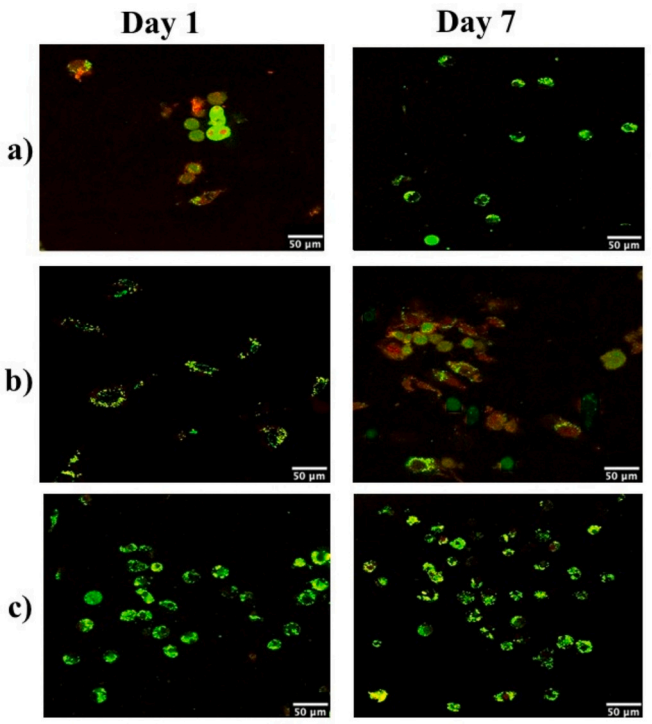

Fig. 13. Fluorescence microscopy images of MC3T3-E1 pre-osteoblasts cultured on (a) uncoated, (b) LbL-coated (uncrosslinked), and (c) TA-crosslinked LbL-coated scaffold types at Day 1 and Day 7. Cell viability was assessed using calcein-AM (green, live cells) and propidium iodide (red, dead cells) staining. Scale bar = 50 µm.

ambient conditions, with a greater than 560% improvement following the deposition of 10 quadlayers. However, under hydrated conditions, a pronounced reduction in mechanical properties was observed, attributable to the plasticising effect of water on the scaffolds [14]. As hydrated environments more closely mimic *in vivo* conditions, various crosslinking strategies have been explored to maintain the mechanical properties of the LbL-coated porous scaffolds under hydrated conditions, enabling them to function under *in vivo* application. This phenomenon has been reported previously, with Acheson et al. showing that glutaraldehyde-crosslinked LbL coatings on open-cell polyurethane foams retained up to 56% of their mechanical properties under hydrated conditions [14]. In the present study, TA crosslinking enabled the scaffolds to retain approximately 75% of their dry-state modulus in PBS at 37 °C, highlighting the effectiveness of TA in mitigating water-induced softening [37]. The improved retention of mechanical properties is likely due to the formation of both hydrogen and covalent bonds between the phenolic hydroxyl groups in the TA and amino acid residues in the LbL coating, as well as hydrophobic and metal-coordination interactions, which collectively increase crosslinking density and stability [37]. This is further supported by Picchio et al. (2018), their study demonstrated improved water resistance and reduced swelling in TA-crosslinked protein films [53].

ATR-FTIR spectra showed an increased intensity and broadening of the bands assigned to -OH, -NH, and methylene groups in the TA-crosslinked coatings, indicating a higher density of interacting functional groups. The spectral changes support the formation of hydrogen bonding between phenolic hydroxyl groups of TA and amine or carboxyl groups of PLL and PGA. In addition, shifts in amide-related bands suggest the formation of covalent linkages, consistent with reactions between oxidised phenolic groups and amine functionalities.

XRD and EDX analyses confirmed the successful incorporation and homogeneous distribution of both MTM nanoclay and TA within the multilayer coatings, contributing to the improved mechanical and physicochemical properties of the LbL-coated scaffolds. The XRD results also suggested enhanced intermolecular packing and increased structural organisation following TA crosslinking. The main diffraction peaks were identified as Na—Si and SiO_2-related phases, consistent with the presence of nanoclay and tannate-associated structures within the coating.

Together, these findings indicate that TA-mediated crosslinking strengthens the multilayer network through combined hydrogen bonding, electrostatic interactions, and covalent bonding, increasing crosslinking density, limiting polymer chain mobility, reducing water-induced plasticisation, and improving coating integrity and mechanical stability under hydrated conditions, enabling them to potentially function under *in vivo* application.

The contact angle measurements demonstrated a substantial increase in hydrophilicity following LbL coating and TA crosslinking, with the water contact angle decreasing from 138.80° (±2.85) for uncoated polyurethane scaffold to 70.28° (±3.10) for TA-crosslinked scaffolds. This increase in hydrophilicity is expected to benefit cell adhesion and proliferation [15].

The *in vitro* degradation study, conducted under dynamic conditions with enzymatic supplementation, provided insights into scaffold stability and degradation kinetics under physiologically relevant conditions [54]. The use of lysozyme and lipase, present in human serum, allowed for a more accurate simulation of the *in vivo* enzymatic environment [54]. Across all scaffold groups, pH remained stable throughout the 56-day degradation period, indicating that scaffold degradation did not induce significant environmental changes. The swelling ratio was reduced in TA-crosslinked scaffolds compared to uncrosslinked and uncoated groups, consistent with the literature on crosslinked networks acting as barriers to water infiltration and reducing chain mobility [14]. The total mass loss after 56 days was lowest for the crosslinked LbL-coated scaffolds (10.50%), confirming that TA crosslinking effectively slowed enzymatic degradation and maintained scaffold integrity. These results align with previous studies reporting that crosslinking can protect polyurethane matrices from rapid enzymatic breakdown, thereby extending their functional lifespan in tissue engineering applications [55].

The preservation of scaffold structure and interconnected porosity during degradation is crucial for nutrient transfer and cellular infiltration, both of which are essential for successful bone regeneration [56]. The degradation behaviour of the TA-crosslinked LbL coating is governed by the crosslinking density and the nature of intermolecular interactions within the multilayer network. Higher crosslink density reduces network permeability, limits water diffusion, and restricts enzymatic access, thereby slowing hydrolytic and enzymatic degradation. In contrast, lower crosslink density increases swelling, enhances mass transport, and accelerates degradation rates [37]. The current findings are consistent with a growing body of literature demonstrating the long-term stability, biocompatibility, and safety of polyurethane open-cell foams in both *in vitro* and *in vivo* models (63–67). For example, Iyer et al. demonstrated that polyurethane foam-based scaffolds successfully integrated into auricular defects in a pig model, supporting their potential for cartilage tissue engineering [57]. Meskinfam et al. showed that polyurethane foam-based scaffolds were suitable for long-term implantation, exhibiting controlled biodegradation without producing cytotoxic by-products, as confirmed by *in vitro* and biomineralisation studies [58]. Graul et al. used imaging techniques to evaluate polyurethane foam-based scaffold degradation in porcine arteries, further confirming the biocompatibility and safety of these materials [59]. Additional studies by Minnen et al. demonstrated the biocompatibility of polyurethane foam-based scaffolds following subcutaneous implantation in a rat model [60], while Vakil et al. reported that highly porous polyurethane foams exhibited favourable biocompatibility in *in vitro* degradation studies, which included both hydrolysis and oxidation processes to better simulate *in vivo* conditions and accurately predict degradation rates before animal studies [61].

The crosslinked network enhances structural integrity, improves surface wettability and enables gradual exposure of bioactive functional groups (–COOH and –NH_2), which promotes protein adsorption and strengthens cell–material interactions, ultimately supporting improved cell attachment and proliferation [38,52]. Biological assessment using MC3T3-E1 pre-osteoblasts demonstrated that all scaffold groups were non-cytotoxic, with cell viabilities exceeding 100% after 48 h of exposure to scaffold extracts, in accordance with ISO 10993-5 [50]. Cell attachment efficiencies were greater than 80% for all groups, with the highest attachment observed on TA-crosslinked scaffolds. The alamarBlue assay indicated that metabolic activity and cell proliferation were greatest in the crosslinked group over 14 days, while uncoated and uncrosslinked scaffolds showed lower proliferation rates. These findings were corroborated by Live/Dead fluorescence imaging and SEM, which showed extensive cell spreading, filopodia formation, and uniform cell layers on the crosslinked scaffolds.

The improved cellular responses observed with TA-crosslinked scaffolds are consistent with previous studies demonstrating that TA can enhance cell viability, attachment, and osteogenic differentiation while avoiding the cytotoxicity associated with glutaraldehyde [36–38]. The combination of improved mechanical stability, reduced degradation, increased hydrophilicity, and enhanced cellular responses underscores the potential of TA-crosslinked LbL-coated polyurethane scaffolds for bone tissue engineering applications [37,52].

The TA-crosslinked LbL nanocomposite scaffold system offers several advantages for tissue engineering applications. Combining LbL nanocomposite coatings with TA crosslinking improves the mechanical stability of highly porous scaffolds under hydrated conditions, which is important for maintaining structural integrity *in vivo*. The use of TA as a naturally derived crosslinker may also reduce cytotoxicity compared with conventional chemical crosslinkers, supporting improved biocompatibility. In addition, the ability to control surface and bulk chemistry, along with degradation behaviour, enables the design of scaffolds that better support cell attachment, proliferation, and tissue formation.

Taken together, this study demonstrated that TA crosslinking of LbL-assembled nanocomposite coatings on highly porous polyurethane foam-based scaffolds yielded scaffolds with enhanced mechanical, chemical, and biological performance under physiologically relevant conditions. These findings support the further development and *in vivo* evaluation of TA-crosslinked LbL scaffolds as promising candidates for bone tissue regeneration. Future work will include advanced *in vitro* studies, such as osteogenic differentiation assays, to further assess the osteogenic potential of the scaffolds and support progression toward *in vivo* bone tissue engineering applications.

5. Conclusions

This study demonstrated that TA crosslinking of LbL-assembled PLL/PGA/PDDA/MTM nanocomposite coatings on highly porous polyurethane foam-based scaffolds is an effective strategy for enhancing scaffold performance in bone tissue engineering. The crosslinked LbL-coated scaffolds exhibited improved mechanical stability under hydrated conditions, reduced swelling, lower water contact angles, and slower degradation rates compared to uncoated and uncrosslinked controls. These modifications were achieved without compromising scaffold porosity or biocompatibility.

In vitro studies with MC3T3-E1 pre-osteoblasts confirmed that the crosslinked scaffolds supported high levels of cell viability, attachment, and proliferation, along with favourable cell morphology. These findings are consistent with and extend previous work on LbL-assembled and crosslinked biomaterial systems, highlighting the added value of TA as a biocompatible crosslinker that addresses the limitations of conventional agents such as glutaraldehyde.

This work provides new insight into the design of robust, multifunctional scaffolds with tuneable properties for bone tissue regeneration. The fabrication protocol developed herein enables the controlled deposition of functional nanocomposite coatings on open-cell polymer-based templates, addressing key challenges related to mechanical integrity and biological response. These results position TA-crosslinked LbL-coated polyurethane foam-based scaffolds as promising candidates for further preclinical evaluation in non-load-bearing bone tissue engineering applications.

CRediT authorship contribution statement

MohammadAli Sahebalzamani: Writing – review & editing, Writing – original draft, Visualization, Validation, Resources, Methodology, Investigation, Formal analysis, Data curation. **John Redmond:** Writing – review & editing, Validation, Investigation, Formal analysis, Data curation. **Srishti Agarwal:** Writing – review & editing, Formal analysis, Data curation. **Helen O. McCarthy:** Writing – review & editing. **Tanya J. Levingstone:** Writing – review & editing, Supervision, Resources, Project administration. **Nicholas J. Dunne:** Writing – review & editing, Supervision, Resources, Project administration, Methodology, Conceptualization.

Declaration of competing interest

The authors declare that they have no known competing financial interests or personal relationships that could have appeared to influence the work reported in this paper.

Acknowledgements

The research conducted in this publication was funded by the Research Ireland (Government of Ireland Scholarship Scheme) under award number GOIPG/2020/1344. The FTIR and contact angle analyses were completed at the Nano Research Facility (NRF) in Dublin City University (DCU), which was funded under the Programme for Research in Third Level Institutions (PRTLI) Cycle 5. The PRTLI is co-funded through the European Regional Development Fund (ERDF), part of the European Union Structural Funds Programme 2011–2015.

Data availability

Data will be made available on request.

References

[1] G. Battafarano, M. Rossi, V. De Martino, F. Marampon, L. Borro, A. Secinaro, et al., Strategies for bone regeneration: from graft to tissue engineering, Int. J. Mol. Sci. 22 (3) (2021) 3, https://doi.org/10.3390/ijms22031128.
[2] E. Chiarello, M. Cadossi, G. Tedesco, P. Capra, C. Calamelli, A. Shehu, et al., Autograft, allograft and bone substitutes in reconstructive orthopedic surgery, Aging Clin. Exp. Res. 25 (Suppl. 1) (2013) S101–S103, https://doi.org/10.1007/s40520-013-0088-8 (PubMed PMID: 24046051).
[3] V. Georgeanu, O. Gingu, I. Antoniac, H. Manolea, Current options and future perspectives on bone graft and biomaterials substitutes for bone repair, from clinical needs to advanced biomaterials research, Appl. Sci. 13 (2023) 8471, https://doi.org/10.3390/app13148471.
[4] M. Selim, H.M. Mousa, G.T. Abdel-Jaber, A. Barhoum, A. Abdal-hay, Innovative designs of 3D scaffolds for bone tissue regeneration: understanding principles and addressing challenges, Eur. Polym. J. 215 (2024) 113251, https://doi.org/10.1016/j.eurpolymj.2024.113251.
[5] A.R. Vaccaro, The role of the osteoconductive scaffold in synthetic bone graft, Orthopedics 25 (5 Suppl) (2002) s571–s578, https://doi.org/10.3928/0147-7447-20020502-05 (PubMed PMID: 12038844).
[6] T. Sadat Hashemi, S. Jaiswal, H.O. McCarthy, T.J. Levingstone, N.J. Dunne, Biofunctionalisation of porous additively manufactured magnesium-based alloys for orthopaedic applications: a review, Biomater. Adv. 169 (2025) 214170, https://doi.org/10.1016/j.bioadv.2024.214170.
[7] K. Gupta, K. Meena, Artificial bone scaffolds and bone joints by additive manufacturing: a review, Bioprinting 31 (2023) e00268, https://doi.org/10.1016/j.bprint.2023.e00268.
[8] P. Gentile, I. Carmagnola, T. Nardo, V. Chiono, Layer-by-layer assembly for biomedical applications in the last decade, Nanotechnology 26 (42) (2015)

422001, https://doi.org/10.1088/0957-4484/26/42/422001 (PubMed PMID: 26421916).
[9] A. Sahebalzamani, M. Ziminska, H. McCarthy, T. Levingstone, N. Dunne, A. Hamilton, Advancing bone tissue engineering one layer at a time: a layer-by-layer assembly approach to 3D bone scaffold materials, Biomater. Sci. 10 (2022), https://doi.org/10.1039/D1BM01756J.
[10] K. Ariga, E. Ahn, M. Park, B.S. Kim, Layer-by-layer assembly: recent Progress from layered assemblies to layered Nanoarchitectonics, Chem. Asian J. 14 (15) (2019) 2553–2566, https://doi.org/10.1002/asia.201900627 (PubMed PMID: 31172648).
[11] A. McFerran, M.J. McIvor, P. Lemoine, B.J. Meenan, J.G. Acheson, Biocompatible nanocomposite coatings deposited via layer-by-layer assembly for the mechanical reinforcement of highly porous interconnected tissue-engineered scaffolds, Bioengineering 9 (10) (2022) 10, https://doi.org/10.3390/bioengineering9100585.
[12] M. Ziminska, N. Dunne, A.R. Hamilton, Porous materials with tunable structure and mechanical properties via templated layer-by-layer assembly, ACS Appl. Mater. Interfaces 8 (34) (2016) 21968–21973, https://doi.org/10.1021/acsami.6b07806 (PubMed PMID: 27513218).
[13] P. Podsiadlo, M. Michel, J. Lee, E. Verploegen, N. Wong Shi Kam, V. Ball, et al., Exponential growth of LBL films with incorporated inorganic sheets, Nano Lett. 8 (6) (2008) 1762–1770, https://doi.org/10.1021/nl8011648.
[14] J.G. Acheson, A. McFerran, D. Xu, M. Ziminska, S. Goel, A.B. Lennon, et al., Hydrated behavior of multilayer polyelectrolyte-nanoclay coatings on porous materials and demonstration of shape memory effect, Surf. Coat. Technol. 458 (2023) 129335, https://doi.org/10.1016/j.surfcoat.2023.129335.
[15] M. Sahebalzamani, T. Sadat Hashemi, Z. Mousavi Nejad, S. Agarwal, H. O. McCarthy, T.J. Levingstone, et al., Deposition of multilayer coatings onto highly porous materials by layer-by-layer assembly for bone tissue engineering applications using cyclic mechanical deformation and perfusion, Mater. Adv. 5 (6) (2024) 2316–2327, https://doi.org/10.1039/D3MA00664F.
[16] M. Ziminska, N. Dunne, A. Hamilton, Customization of mechanical properties and porosity of bone tissue scaffold materials via layer-by-layer assembly of polymer-nanocomposite coatings, MRS Online Proc. Libr. 1793 (1) (2015) 67–72, https://doi.org/10.1557/opl.2015.827.
[17] M. Zanetta, N. Quirici, F. Demarosi, M.C. Tanzi, L. Rimondini, S. Farè, Ability of polyurethane foams to support cell proliferation and the differentiation of MSCs into osteoblasts, Acta Biomater. 5 (4) (2009) 1126–1136, https://doi.org/10.1016/j.actbio.2008.12.003.
[18] S.M. Giannitelli, F. Basoli, P. Mozetic, P. Piva, F.N. Bartuli, F. Luciani, et al., Graded porous polyurethane foam: a potential scaffold for oro-maxillary bone regeneration, Mater. Sci. Eng. C 51 (2015) 329–335, https://doi.org/10.1016/j.msec.2015.03.002.
[19] R. Sahoo, A.S. Sanket, A. Pattnaik, S. Pany, S. Pradhan, S. Pati, et al., Designing of porous scaffolds for tissue engineering and regenerative medicine, J. Mater. Chem. B 14 (9) (2026) 2733–2773, https://doi.org/10.1039/D5TB02507A.
[20] M.H. Dzulkifli, M.Y. Yahya, R.A. Majid, Fire retardancy, thermal, and physico-mechanical properties of semi-rigid water-blown polyurethane foam from palm oil-based polyol, Cell. Polym. 41 (3) (2022) 103–118, https://doi.org/10.1177/02624893211061633.
[21] J. Acheson, M. Ziminska, S. Goel, N. Dunne, A. Hamilton, Effect of Hydration on the Mechanical Behaviour of Nanocomposite-coated Porous Bone Scaffold Materials: United Kingdom Society of Biomaterials, 2015.
[22] W.J. Seo, H.C. Jung, J.C. Hyun, W.N. Kim, Y.B. Lee, K.H. Choe, et al., Mechanical, morphological, and thermal properties of rigid polyurethane foams blown by distilled water, J. Appl. Polym. Sci. 90 (1) (2003) 12–21, https://doi.org/10.1002/app.12238.
[23] X. Feng, R. Pelton, M. Leduc, Mechanical properties of polyelectrolyte complex films based on polyvinylamine and carboxymethyl cellulose, Ind. Eng. Chem. Res. 45 (20) (2006) 6665–6671, https://doi.org/10.1021/ie060511f.
[24] A.J. Nolte, N.D. Treat, R.E. Cohen, M.F. Rubner, Effect of relative humidity on the young's Modulus of polyelectrolyte multilayer films and related nonionic polymers, Macromolecules 41 (15) (2008) 5793–5798, https://doi.org/10.1021/ma800732j.
[25] L. Zhou, D. Liang, X. He, J. Li, H. Tan, J. Li, et al., The degradation and biocompatibility of pH-sensitive biodegradable polyurethanes for intracellular multifunctional antitumor drug delivery, Biomaterials 33 (9) (2012) 2734–2745, https://doi.org/10.1016/j.biomaterials.2011.11.009.
[26] Q. An, T. Huang, F. Shi, Covalent layer-by-layer films: chemistry, design, and multidisciplinary applications, Chem. Soc. Rev. 47 (13) (2018) 5061–5098, https://doi.org/10.1039/C7CS00406K.
[27] Y.H. Yang, L. Bolling, M. Haile, J.C. Grunlan, Improving oxygen barrier and reducing moisture sensitivity of weak polyelectrolyte multilayer thin films with crosslinking, RSC Adv. 2 (32) (2012) 12355, https://doi.org/10.1039/c2ra21845c.
[28] H.H. Hariri, A.M. Lehaf, J.B. Schlenoff, Mechanical properties of osmotically stressed polyelectrolyte complexes and multilayers: water as a plasticizer, Macromolecules 45 (23) (2012) 9364–9372, https://doi.org/10.1021/ma302055m.
[29] Z. Eslami, S. Elkoun, M. Robert, K. Adjallé, A review of the effect of plasticizers on the physical and mechanical properties of alginate-based films, Molecules 28 (18) (2023), https://doi.org/10.3390/molecules28186637.
[30] Z. Wang, H. Liu, W. Luo, T. Cai, Z. Li, Y. Liu, et al., Regeneration of skeletal system with genipin crosslinked biomaterials, J. Tissue Eng. 11 (2020) 2041731420974861, https://doi.org/10.1177/2041731420974861.
[31] H.C. Liang, W.H. Chang, H.F. Liang, M.H. Lee, H.W. Sung, Crosslinking structures of gelatin hydrogels crosslinked with genipin or a water-soluble carbodiimide, J. Appl. Polym. Sci. 91 (6) (2004) 4017–4026, https://doi.org/10.1002/app.13563.
[32] M. Ziminska, M.J. Chalanqui, P. Chambers, J.G. Acheson, H.O. McCarthy, N. J. Dunne, et al., Nanocomposite-coated porous templates for engineered bone scaffolds: a parametric study of layer-by-layer assembly conditions, Biomed. Mater. 14 (6) (2019) 065008, https://doi.org/10.1088/1748-605X/ab3b7b (PubMed PMID: 31539364).
[33] T. Haghparast-Kenarsari, M. Abdouss, S. Heidari Keshel, Z. Heshmatipour, A. Rahimi, E. Biazar, Improving properties of platelet-rich fibrin scaffold with tannic acid for wound healing, Int. Wound J. 21 (4) (2024) e14571, https://doi.org/10.1111/iwj.14571 (PubMed PMID: 38111169; PubMed Central PMCID: PMC10961897).
[34] D. Scheffel, L. Bianchi, D. Soares, F. Basso, C. Sabatini, C. de Souza Costa, et al., Transdentinal cytotoxicity of carbodiimide (EDC) and glutaraldehyde on odontoblast-like cells, Oper. Dent. 40 (1) (2015) 44–54, https://doi.org/10.2341/13-338-L.
[35] J.E. Gough, C.A. Scotchford, S. Downes, Cytotoxicity of glutaraldehyde crosslinked collagen/poly(vinyl alcohol) films is by the mechanism of apoptosis, J. Biomed. Mater. Res. 61 (1) (2002) 121–130, https://doi.org/10.1002/jbm.10145.
[36] J. Lee, M. Yeo, W. Kim, Y. Koo, G.H. Kim, Development of a tannic acid cross-linking process for obtaining 3D porous cell-laden collagen structure, Int. J. Biol. Macromol. 110 (2018) 497–503, https://doi.org/10.1016/j.ijbiomac.2017.10.105. Biological Macromolecules for Delivery, Imaging & Therapy (BMDIT-2018).
[37] S.Y.Z. Moghaddam, E. Biazar, J. Esmaeili, B. Kheilnezhad, F. Goleij, S. Heidari, Tannic acid as a green cross-linker for biomaterial applications, Mini Rev. Med. Chem. 23 (13) (2023) 1320–1340, https://doi.org/10.2174/1389557522666220622112959.
[38] A. Baldwin, B.W. Booth, Biomedical applications of tannic acid, J. Biomater. Appl. 36 (8) (2022) 1503–1523, https://doi.org/10.1177/08853282211058099.
[39] H.G. Nam, M.G. Nam, P.J. Yoo, J.H. Kim, Hydrogen bonding-based strongly adhesive coacervate hydrogels synthesized using poly(N-vinylpyrrolidone) and tannic acid, Soft Matter 15 (4) (2019) 785–791, https://doi.org/10.1039/C8SM02144A.
[40] M. Sahebalzamani, H.O. McCarthy, T.J. Levingstone, N.J. Dunne, Systematic design and optimisation of layer-by-layer nanocomposite coatings on three-dimensional porous scaffolds for enhanced mechanical performance in bone tissue engineering applications, RSC Adv. 16 (14) (2026) 12389–12407, https://doi.org/10.1039/D5RA09314G.
[41] P. Chidchai, K. Singpanna, S. Pengnam, T. Charoenying, B. Pamornpathomkul, P. Patrojanasophon, et al., Experimental optimization of tannic acid-crosslinked hydrogels for neomycin delivery in infected wounds, Polymers 17 (6) (2025) 770, https://doi.org/10.3390/polym17060770.
[42] L.J. Gibson, M.F. Ashby, The mechanics of three-dimensional cellular materials, Proc. R. Soc. Lond. A Math. Phys. Sci. 382 (1782) (1982) 43–59.
[43] A.D. Gholap, S. Rojekar, H.S. Kapare, N. Vishwakarma, S. Raikwar, A. Garkal, et al., Chitosan scaffolds: expanding horizons in biomedical applications, Carbohydr. Polym. 323 (2024) 121394, https://doi.org/10.1016/j.carbpol.2023.121394 (PubMed PMID: 37940287).
[44] Y. Yuan, B.M. Chesnutt, L. Wright, W.O. Haggard, J.D. Bumgardner, Mechanical property, degradation rate, and bone cell growth of chitosan coated titanium influenced by degree of deacetylation of chitosan, J Biomed Mater Res B Appl Biomater 86B (1) (2008) 245–252, https://doi.org/10.1002/jbm.b.31012.
[45] E.V. Melnik, S.N. Shkarina, S.I. Ivlev, V. Weinhardt, T. Baumbach, M.V. Chaikina, et al., *In vitro* degradation behaviour of hybrid electrospun scaffolds of polycaprolactone and strontium-containing hydroxyapatite microparticles, Polym. Degrad. Stab. 167 (2019) 21–32, https://doi.org/10.1016/j.polymdegradstab.2019.06.017.
[46] J. Redmond, H. McCarthy, P. Buchanan, T.J. Levingstone, N.J. Dunne, Advances in biofabrication techniques for collagen-based 3D *in vitro* culture models for breast cancer research, Mater. Sci. Eng. C 122 (2021) 111944, https://doi.org/10.1016/j.msec.2021.111944.
[47] C. Yang, Enhanced physicochemical properties of collagen by using EDC/NHS-crosslinking, Bull. Mater. Sci. 35 (5) (2012) 913–918, https://doi.org/10.1007/s12034-012-0376-5.
[48] Y.M. Li, X. Miao, Z.G. Wei, J. Cui, S.Y. Li, R. Han, et al., Iron-tannic acid nanocomplexes: facile synthesis and application for removal of methylene blue from aqueous solution 11 (2016) 1045–1061.
[49] J. Iglesias, E. García de Saldaña, J.A. Jaén, On the tannic acid interaction with metallic iron, Hyperfine Interact. 134 (1) (2001) 109–114, https://doi.org/10.1023/A:1013838600599.
[50] Biological evaluation of medical devices—Part 1: evaluation and testing within a risk management process, in: ANSI/AAMI/ISO 10993-1:2018; Biological evaluation of medical devices—Part 1: Evaluation and Testing Within A Risk Management Process, AAMI, 2020 [cited 2024 Jul 29]. Available from: http://array.aami.org/doi/10.2345/9781570207556.ch1 doi:10.2345/9781570207556.ch1.
[51] K.M. Percival, V. Paul, G.A. Husseini, Recent advancements in bone tissue engineering: integrating smart scaffold technologies and bio-responsive systems for enhanced regeneration, Int. J. Mol. Sci. 25 (11) (2024) 11, https://doi.org/10.3390/ijms25116012.
[52] V. Acharya, A. Ghosh, A.R. Chowdhury, P. Datta, Tannic acid-crosslinked chitosan matrices enhance osteogenic differentiation and modulate epigenetic status of cultured cells over glutaraldehyde crosslinking, Soft Mater. 20 (2) (2022) 149–160, https://doi.org/10.1080/1539445X.2021.1933032.
[53] M.L. Picchio, Y.G. Linck, G.A. Monti, L.M. Gugliotta, R.J. Minari, C.I. Alvarez Igarzabal, Casein films crosslinked by tannic acid for food packaging applications,

Food Hydrocoll. 84 (2018) 424–434, https://doi.org/10.1016/j.foodhyd.2018.06.028.
[54] A.R. Costa-Pinto, A.M. Martins, M.J. Castelhano-Carlos, V.M. Correlo, P.C. Sol, A. Longatto-Filho, et al., In vitro degradation and in vivo biocompatibility of chitosan–poly(butylene succinate) fiber mesh scaffolds, J. Bioact. Compat. Polym. 29 (2) (2014) 137–151, https://doi.org/10.1177/0883911514521919.
[55] E. Marten, R.J. Müller, W.D. Deckwer, Studies on the enzymatic hydrolysis of polyesters. II. Aliphatic–aromatic copolyesters, Polym. Degrad. Stab. 88 (3) (2005) 371–381, https://doi.org/10.1016/j.polymdegradstab.2004.12.001.
[56] K.S. Ogueri, T. Jafari, J.L. Escobar Ivirico, C.T. Laurencin, Polymeric biomaterials for scaffold-based bone regenerative engineering, Regen. Eng. Transl. Med. 5 (2) (2019) 128–154, https://doi.org/10.1007/s40883-018-0072-0 (PubMed PMID: 31423461; PubMed Central PMCID: PMC6697158).
[57] K. Iyer, B.L. Dearman, M.J.D. Wagstaff, J.E. Greenwood, A novel biodegradable polyurethane matrix for auricular cartilage repair: an in vitro and in vivo study, J. Burn Care Res. 37 (4) (2016) e353–e364, https://doi.org/10.1097/BCR.0000000000000281.
[58] M. Meskinfam, S. Bertoldi, N. Albanese, A. Cerri, M.C. Tanzi, R. Imani, et al., Polyurethane foam/nano hydroxyapatite composite as a suitable scaffold for bone tissue regeneration, Mater. Sci. Eng. C 82 (2018) 130–140, https://doi.org/10.1016/j.msec.2017.08.064.
[59] L.M. Graul, S.J. Horn, L.D. Nash, T.B. Cheung, F.J. Clubb, D.J. Maitland, Image-based evaluation of in vivo degradation for shape-memory polymer polyurethane foam, Polymers 14 (19) (2022) 19, https://doi.org/10.3390/polym14194122.
[60] B. van Minnen, M.B.M. van Leeuwen, B. Stegenga, J. Zuidema, C.E. Hissink, T. G. van Kooten, et al., Short-term in vitro and in vivo biocompatibility of a biodegradable polyurethane foam based on 1,4-butanediisocyanate, J. Mater. Sci. Mater. Med. 16 (3) (2005) 221–227, https://doi.org/10.1007/s10856-005-6683-2 (PubMed PMID: 15744613).
[61] A.U. Vakil, N.M. Petryk, C. Du, B. Howes, D. Stinfort, S. Serinelli, et al., In vitro and in vivo degradation correlations for polyurethane foams with tunable degradation rates, J. Biomed. Mater. Res. A 111 (5) (2023) 580–595, https://doi.org/10.1002/jbm.a.37504 (PubMed PMID: 36752708).